SUPPLEMENTARY INFORMATION

Nanocellulose films with multiple functional nanoparticles in confined spatial distribution

Soledad Roig-Sanchez[a], Erik Jungstedt[b], Irene Anton-Sales[a], David C. Malaspina[a], Jordi Faraudo[a], Lars Berglund[b], Anna Laromaine[a], Anna Roig[a]*

[a] *Institut de Ciència de Materials de Barcelona (ICMAB), Campus UAB, Bellaterra, Catalonia, E-08193, Spain*
[b] *Department of Fiber and Polymer Technology, Wallenberg Wood Science Center, Royal Institute of Technology (KTH), SE-100 44 Stockholm, Sweden*
E-mail: roig@icmab.es

EXPERIMENTAL SECTION

1. Materials

The bacteria strain *Komagataeibacter xylinus* (*K. xylinus*) (NCIMB 5346) was purchased from CECT (Valencia, Spain). The culture media was prepared using glucose, peptone, yeast extract and agar (Conda Lab), $Na_2HPO_4 \cdot 12H_2O$ and citrate acid monohydrate (Sigma-Aldrich). For the cleaning process, a solution of NaOH (Sigma-Aldrich) 0.1M was used.

For the nanoparticle synthesis, iron(III) acetylacetonate ($Fe(acac)_3$, 97%), titanium(IV) butoxide (TBOT, 97%), oleyamine (OA, 70%), polyvinylpyrrolidone (PVP, molecular weight 10k) and gold(III) chloride hydrate ($HAuCl_4$) were purchased from Sigma-Aldrich. Silver nitrate ($AgNO_3$) was purchased from Panreac and benzyl alcohol (BA, 99%) from Scharlau.

2. Production of Bacterial Cellulose Films

K. xylinus bacteria was grown in Hestrin-Schramm solid medium (1.15 g citric acid, 6.8 g $Na_2HPO_4 \cdot 12H_2O$, 5 g peptone, 5 g yeast, 15 g agar and 20 g dextrose per liter). A colony was expanded in 6 mL of the same liquid medium (i.e without agar) for 7 days at 30 ˚C. After that, 0.5 mL were inoculated into 4.5 mL of fresh liquid medium and incubated for another three days. Finally, a dilution of the bacterial solution with fresh medium was done in a proportion 1:14, transferred into 24 well-plates and kept for 3 days inside an incubator. Then, the bacterial cellulose (BC) films formed on top of the liquid in each well (diameter ≈ 1.5 cm) were harvested and soaked in a solution 1:1 EtOH:Milli-Q (MQ) water for 10 min, boiled twice in MQ water for 20 min and another two times, for 20 min, in a 0.1 M NaOH solution to remove organic residues. After the alkali treatment, BC films were washed with MQ water until neutral pH was reached and were stored in water at room temperature until further use. After drying at 60 ˚C degrees, a typical BC film presents a density of ~ 0.7 g/cm^3 and a porosity of ~ 53 %.

3. Synthesis of Bacterial Cellulose Nanocomposites

Nanoparticles (NPs) were *in situ* synthesized in never dried BC films using a microwave oven with controlled atmosphere (CEM Discover Explorer-12 Hybrid reactor operating at a frequency of 2.45 GHz and with a maximum power of 300 W). Temperature and time were specifically set for each reaction while the power was automatically adjusted to heat the sample using a volume-independent infrared sensor that controls the temperature and pressure inside the reaction vessel. After the reaction, the samples were cooled down to 50 ˚C with compressed air.

Before the syntheses, the cellulose films were immersed in benzyl alcohol for 12 h to assure a complete exchange of solvent. This step was not necessary for the silver nanoparticles reaction, which takes place in water.

The BC/Fe_2O_3 was fabricated by previously mixing 0.35mmol (123.6 mg) $Fe(acac)_3$ in 4.5mL benzyl alcohol. Then, a BC film was immersed in the solution and heated in two steps: 1) 5 min at 60 ˚C and 2) 10 min at 210 ˚C.[1] Cellulose containing titania NPs (BC/TiO_2) was obtained mixing 14 µL TBOT (0.04 mmol) in 4 mL of benzyl alcohol and also heating in two steps: 1) 5 min at 50 ˚C 2) 10 min at 190 ˚C. Gold NPs cellulose (BC/Au) was obtained by mixing 26 µL of $HAuCl_4$ 250 mM in 1mL of oleyamine and sonicating until complete dissolution. Then, the sample was heated at 120 ˚C for 5 min. Silver NPs cellulose (BC/Ag) was synthesized adding 2 mL of a 25 mM $AgNO_3$ solution to a 2 mL 25 mM PVP 10 K solution, sonicating 5 min and heating at 120 ˚C during 10 min. In all cases, the BC films were added to the solution just before heating.

The BC/nanoparticles films were harvested and cleaned 10 minutes in acetone under gentle agitation two times. Ethanol was used in the case of the gold reaction that uses oleyamine as it dissolves better the excess of solvent in the cellulose. Afterwards, the cellulose nanocomposed films were cleaned with Milli-Q water until complete exchange of solvent and stored at room temperature.

The excess of NPs in the suspension was collected by centrifugation: 1) at 6000 rpm for 30 min using acetone and 20 µL TMAOH as an electrostatic surfactant for Fe_2O_3 NPs. 2) At 6000 rpm for 20 min using acetone and 20 µL TMAOH as an electrostatic surfactant for titania NPs. 3) At 6000 rpm for 15 min using ethanol for Au NPs. 4) At 6000 rpm for 15 min using acetone and 10 µL PVP as an electrostatic surfactant for Ag NPs. This step was repeated twice by redispersing the precipitate. Finally, the particles were dried overnight in an oven at 60˚C and stored in Milli-Q water with 10 µL of surfactant.

For the bilayers and multifeuille constructs, cellulose nanocomposed films were placed one above another in the desired order between two PTFE (polytetrafluoroethylene) plates and were dried at 60 ˚C.

4. Scanning Electron Microscopy (SEM)

BC film samples were fixed on top an aluminum SEM holder with adhesive carbon tape. For the cross-section images, the multilayer construction was cut with a blade (Personna GEM single edge, 3-facet stainless steel, PTFE coated blade, 0.23mm) in order to obtain a clean cut and was placed in a holder with an 90˚ tilt. FEI Quanta 650FEG ESEM was used under low vacuum condition, with an acceleration voltage of 20 kV, an electron beam spot of 4-5 and a working distance of 10 mm for the cross-sections images of the multilayer constructions and the energy-dispersive x-ray (EDX) scan through them. A high-resolution scanning electron microscope (FEI Magellan 400L XHR SEM, ICN2) was used under high vacuum with an acceleration voltage of 2kV, a current of 0.10nA, a working distance of 5 mm and a vCD detector for seeing the nanoparticles distribution on the cellulose fibers.

5. Transmission electron microscopy (TEM)

JEOL JEM-1210 electron microscope operating at 120 kV with an ORIUS 831 SC 600, Gatan camera was used to obtain TEM images and diffraction patterns of the nanoparticles by the selected area electron diffraction (SAED) mode. The nanoparticles mean size was calculated by fitting a histogram of 300-400 nanoparticles to a Gaussian function. Polydispersity (PDI) value was calculated as the percentage of standard deviation/mean value.

6. Thermogravimetric Analysis (TGA)

A TGA-DSC/DTA analyzer (NETZSCH STA 449 F1 Jupiter) with a heating rate of 10 ˚C min^{-1} from room temperature to 800 ˚C in air was used to evaluate the inorganic NP mass and volume fraction in each nanocomposite film. Half of the same films were immersed in 8 mL Milli-Q water during 30 days under gentle horizontal agitation conditions and another TGA was run to monitor particle leaching from the cellulose after that time.

7. UV-VIS spectroscopy

After drying the films, their optical transmittance was measured by a Varian Cary 5000 spectrophotometer in the range between 200 and 800 nm. The samples were placed between an opaque holder with an aperture in the middle and a cover glass, which was fixed with tape to the holder to assure the completely immobilization of the sample.

8. Superconducting quantum interference device (SQUID)

The bacterial cellulose with iron oxide nanoparticles was characterized by measuring its magnetization *versus* an applied magnetic field at 300K in a Quantum Design MPMS-XL equipment.

9. Dynamic mechanical analysis (DMA)

For the peeling test, two BC films were dried at 60 ˚C degrees. A spacing material to which the cellulose does not adhere was added in between both films, covering half of the surface. After drying, the samples were cut using a blade. The final dimensions of the sticking area were 5 mm in width and 7.5 mm in length. The two not-adherent ends of the strip were each glued between two 1.5 cm x 1.5 cm pieces of paper and placed between clamps. This is done to avoid the clamps from damaging the BC films, leading to fail within the griping zone of the test specimen. A displacement sensor was used to move both ends at a constant speed of 0.69 mm/s. The tests were conducted using a linear variable differential transformer and an ADMET load cell of 100 N under controlled temperature and humidity conditions (23±1 ˚C and 25±1 % humidity). The force needed as a function of the displacement was recorded and the area below the curve normalized by the peel off area of the sample (37.5 mm^2) was calculated as the peeling energy needed to separate the two BC pieces. The tests were recorded by a Leica M205FA microscope.

10. All atomic Molecular dynamics (MD) simulations

The molecular dynamics (MD) simulations reported here were performed using the NAMD 2.12 software[2] with a Langevin thermostat at 298 K. In the simulations with water solvent, we also employ a barostat (Langevin piston) at 1 bar. Cellulose fibrils were build using cellulose builder toolkit[3] and described using the carbohydrate section of the CHARMM force field.[4] We have performed MD simulations in dry conditions (no water) and in wet conditions (full hydration). In our simulations in wet conditions, water was described employing the TIP4P/2005 model,[5,6] which best capture hydrogen-bonding features of liquid water at all pressures.[7] We performed minimization, equilibration and production runs (20 ns) of two cellulose fibrils interacting in vacuum and in water. Simulations are periodic in all directions obtaining in that way results similar to infinite long fibrils in the y direction. The force analysis was performed with biased molecular dynamics simulations, using two different methods (due to the different strength of the interactions in the dry and wet cases). For fibrils in vacuum we used Steered Molecular Dynamics (SMD) method to measure the adhesion force, while for the fibrils in water we used Adaptive Biasing Force (ABF) method.[8]. In all simulations Newton's equation of motion were integrated every 2 fs and electrostatic interactions updated every 4 fs. All bonds between heavy atoms and hydrogen atoms were maintained rigid using rigid bonds. Lennard-Jones interactions were computed with a cutoff of 1.2 nm and a switching distance of 1.0 nm. For long range electrostatics we used Particle Mesh Ewald (PME) algorithm using a grid spacing of 1.0 nm. The system considered in the NVT simulations of adhesion of dry fibrils consisted of 2 fibrils of length 6.32 nm with an hexagonal cross section as shown in Figure 3a and. It contains 82556 atoms inside a large simulation box of dimensions 7.86 nm x 6.32 nm x 13.68 nm. The NPT simulations in wet conditions contained the same fibrils inside a simulation box with 16103 water molecules (equilibrium box size after

pressurization at 1 atm is 7.86 nm x 6.32 nm x 12.47 nm). Biased SMD simulations pulling apart the two fibrils were performed starting from an equilibrated configuration with the two fibrils in contact obtained in the NVT dry simulations. The employed force constant was 2000 kcal/mol. Separation speeds of 0.1 nm/ns and 1 nm/ns were employed, giving identical results except by small statistical fluctuations. Biased ABF simulations pulling apart the two fibrils were performed starting from an equilibrated configuration of two hydrated fibrils in contact as obtained from NPT simulations. The employed force constant was 50.0 kcal/mol and the generalized coordinate was the center of mass separation between fibrils.

11. Confocal Microscope

For characterization with confocal microscope, a bilayer BC/Ag-BC/TiO2 was stained with 1 mL of Safranin-O (Alfa Aesar) (1% aqueous solution) overnight in a 24-well plate. Then, the film was rinsed with Milli-Q water several times. After removing the excess water, the wet samples were placed on a IBIDI glass bottom dish and multiple stack images were taken with a Leica SP5 confocal microscope. Safranin-O was exited with an argon laser at λ=488nm at 10X magnification. 3D reconstructions and image processing was performed with ImageJ-Fiji software.

SUPPLEMENTARY FIGURES AND TABLES

Table S1. Nanoparticles synthesis: proposed mechanisms and strategy to vary the inorganic weight fraction.

BC/Au

Schematics

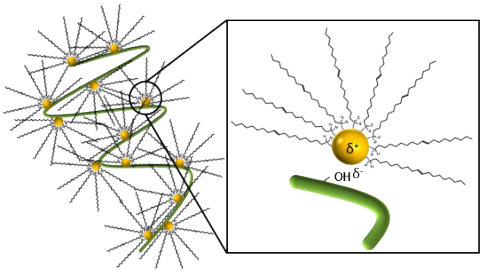

Proposed synthesis mechanism [9]

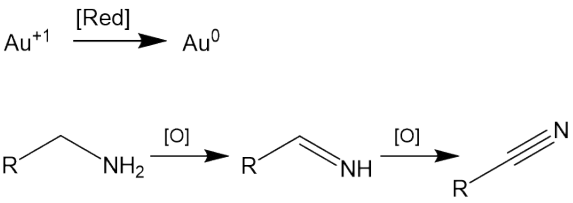

Modification of the nanoparticle loading in the BC/Au composite

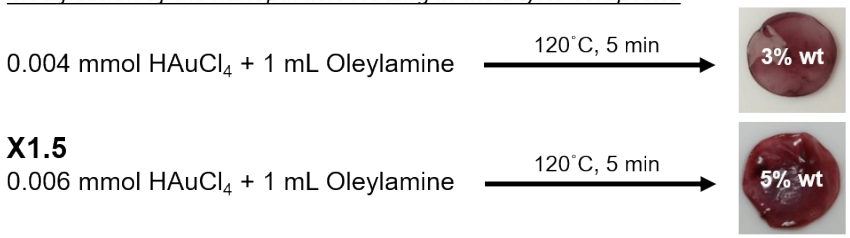

BC/Ag

Schematics

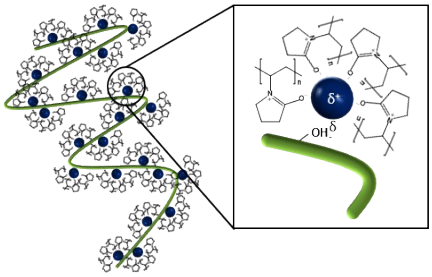

Proposed synthesis mechanism [10,11]

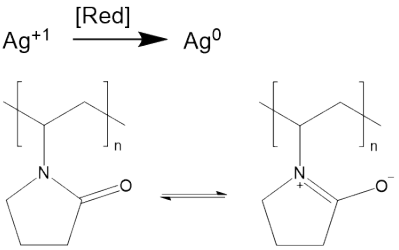

Modification of the nanoparticle loading in the BC/Ag composite

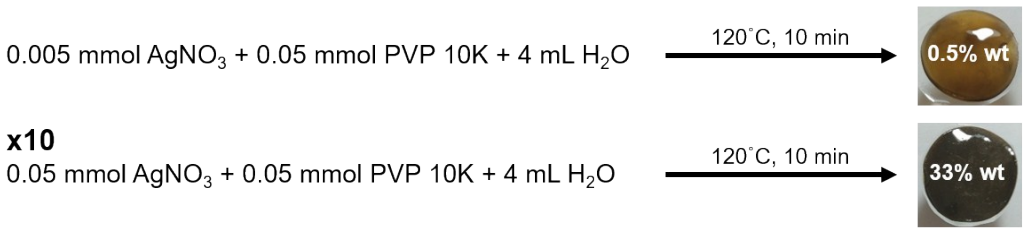

BC/Fe_2O_3

Schematics

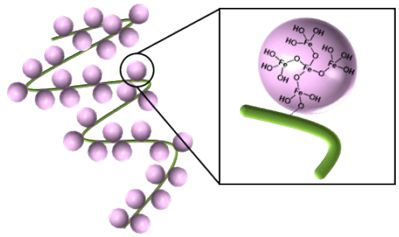

Proposed synthesis mechanism [12]

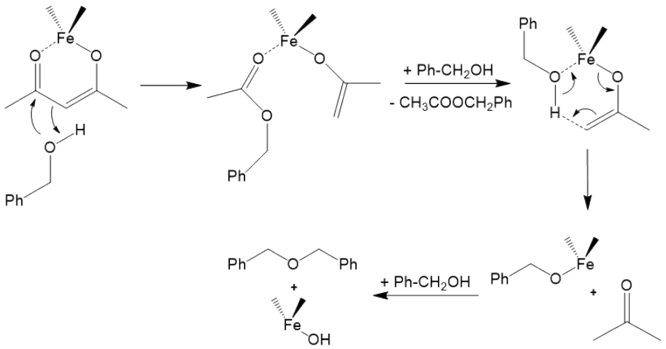

+ condensation

$=Fe\text{-}OH + HO\text{-}Fe= \rightarrow =Fe\text{-}O\text{-}Fe= + H_2O$

$=Fe\text{-}OH + HO\text{-}BC \rightarrow =Fe\text{-}O\text{-}BC + H_2O$

Nanoparticle loading in the BC/Fe_2O_3 composite

0.35 mmol $Fe(acac)_3$ + 4.5 mL Benzylalcohol [1] → (60°C, 5 min; 210°C, 10 min) → 

BC/TiO_2

Schematics

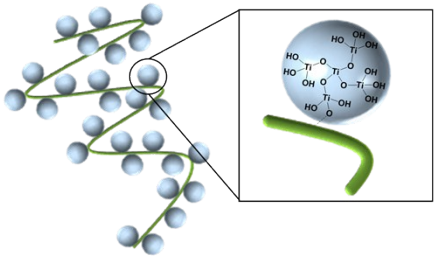

Proposed synthesis mechanism [12,13]

1) $\equiv Ti\text{-}OBut + H_2O \rightarrow \equiv Ti\text{-}OH + ButOH$

2a) $\equiv Ti\text{-}OH + HO\text{-}Ti\equiv \rightarrow \equiv Ti\text{-}O\text{-}Ti\equiv + H_2O$

2b) $\equiv Ti\text{-}OBut + HO\text{-}Ti\equiv \rightarrow \equiv Ti\text{-}O\text{-}Ti\equiv + ButOH$

2c) $\equiv Ti\text{-}OBut + HO\text{-}CH_2\text{-}Ph\equiv \rightarrow \equiv Ti\text{-}O\text{-}Ti\equiv + Ph\text{-}CH_2\text{-}ButOH$

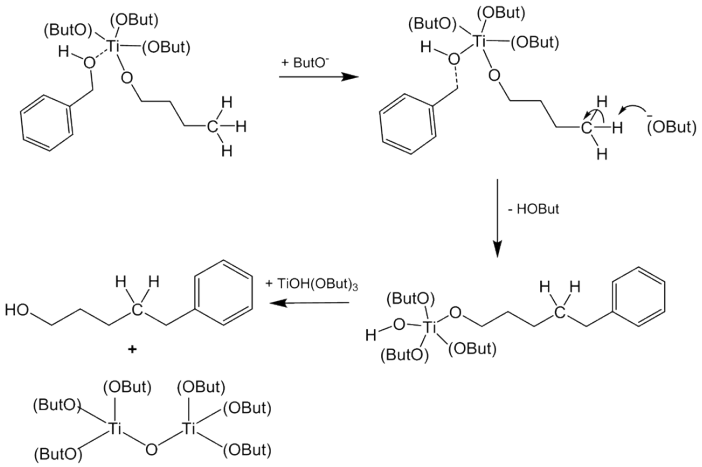

2d) $\equiv Ti\text{-}OBut + HO\text{-}BC \rightarrow \equiv Ti\text{-}O\text{-}BC + ButOH$

2e) $\equiv Ti\text{-}OH + HO\text{-}BC \rightarrow \equiv Ti\text{-}O\text{-}BC + H_2O$

Nanoparticle loading in the BC/TiO_2 composite

0.04 mmol $Ti(OBu)_4$ + 4 mL Benzylalcohol → (50°C, 5 min; 190°C, 10 min) → 

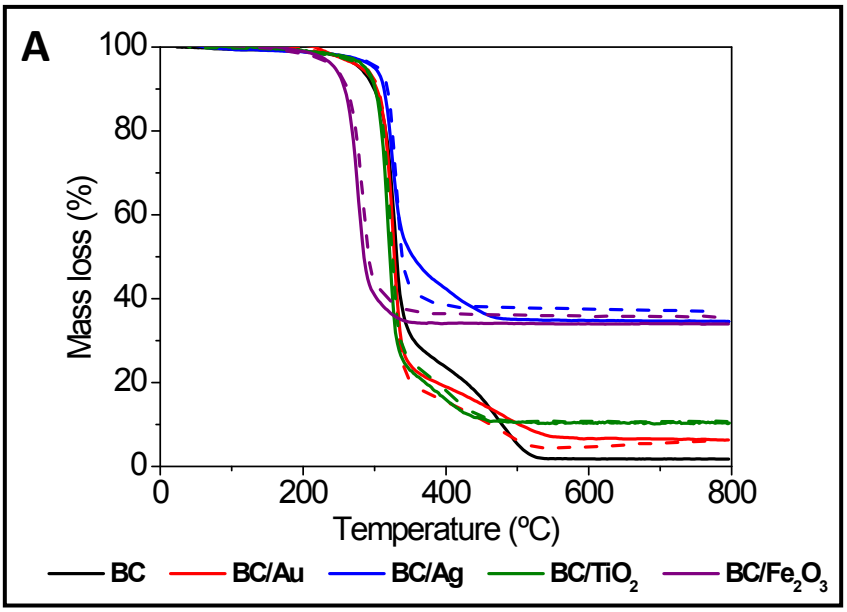

B	BC/Au	BC/Ag	BC/TiO_2	BC/Fe_2O_3
NP loading fraction (wt%)	5 %	33 %	9 %	32 %
NP loading fraction after 1 month in water (wt%)	4 %	35 %	9 %	34 %

Figure S1. A) Thermal gravimetric analysis (TGA) of pristine BC (black line) and nanocomposited BC films (solid color lines). The highest load of nanoparticles (remaining mass in the TGA) is observed for Fe_2O_3 and Ag, while the lowest amount is seen for Au. The loading percentages are in accordance with the precursors ratios used in each synthesis, being 10 times higher for Ag and Fe_2O_3 than for Au and TiO_2. The dotted lines represent the TGA analysis of the BC/nanoparticles films after they have been immersed in water under gentle agitation for 30 days. The nanoparticles fraction remains constant, therefore no leaching of the nanoparticles is observed within the experimental error of the technique. B) Percentages of the mass remaining from the BC/nanocomposites obtained from TGA.

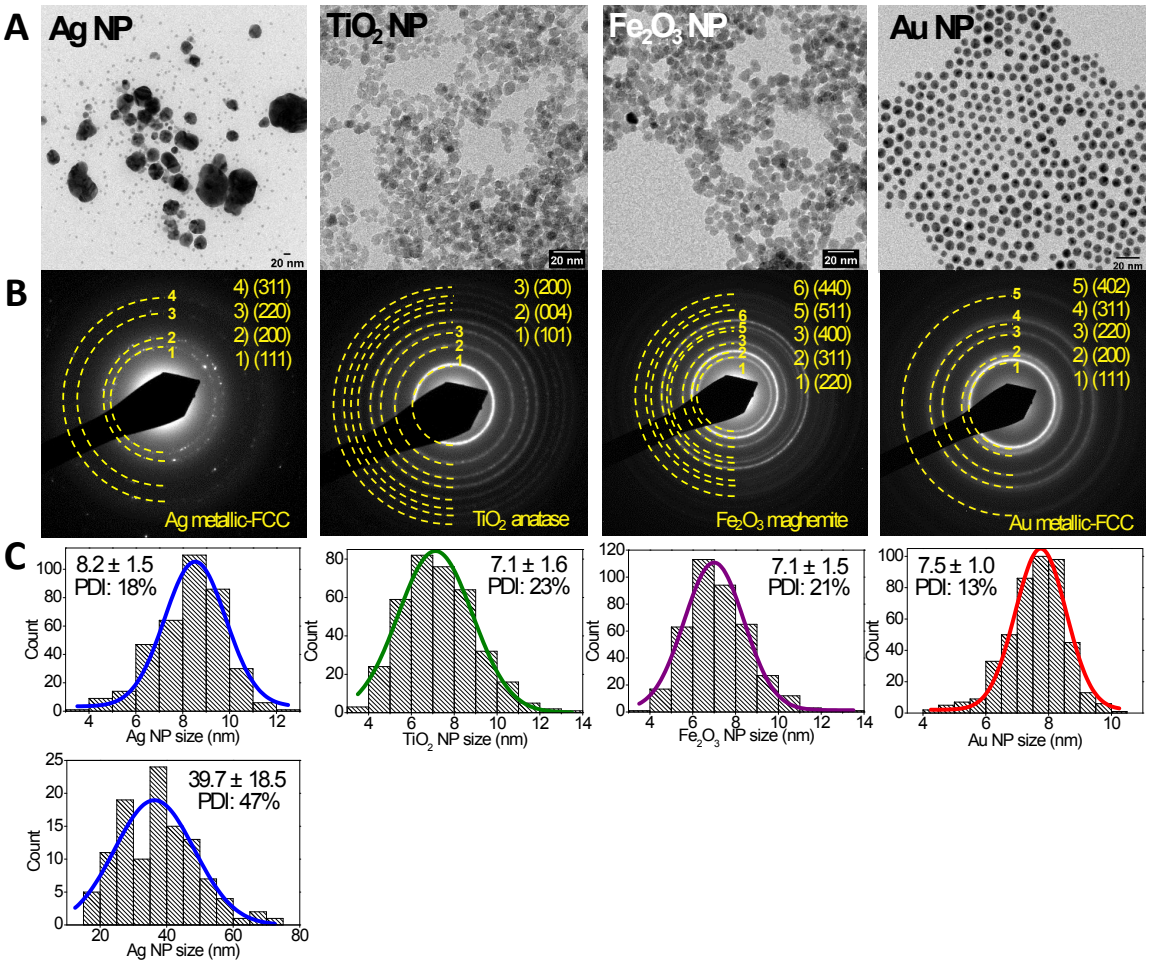

Figure S2. A) TEM images of the synthesized nanoparticles collected from the supernatant. B) SAED images of the different nanoparticles: crystal structure of metallic gold and silver, anatase phase for titania and maghemite for iron oxide are shown. Each characteristic crystallographic planes are highlighted. C) Particle size distribution computed from the TEM images. Two different populations are observed for silver NPs.

Figure S3. BC/BC peeling test video which corresponds to the force *vs* displacement curve showed in Fig 2C.

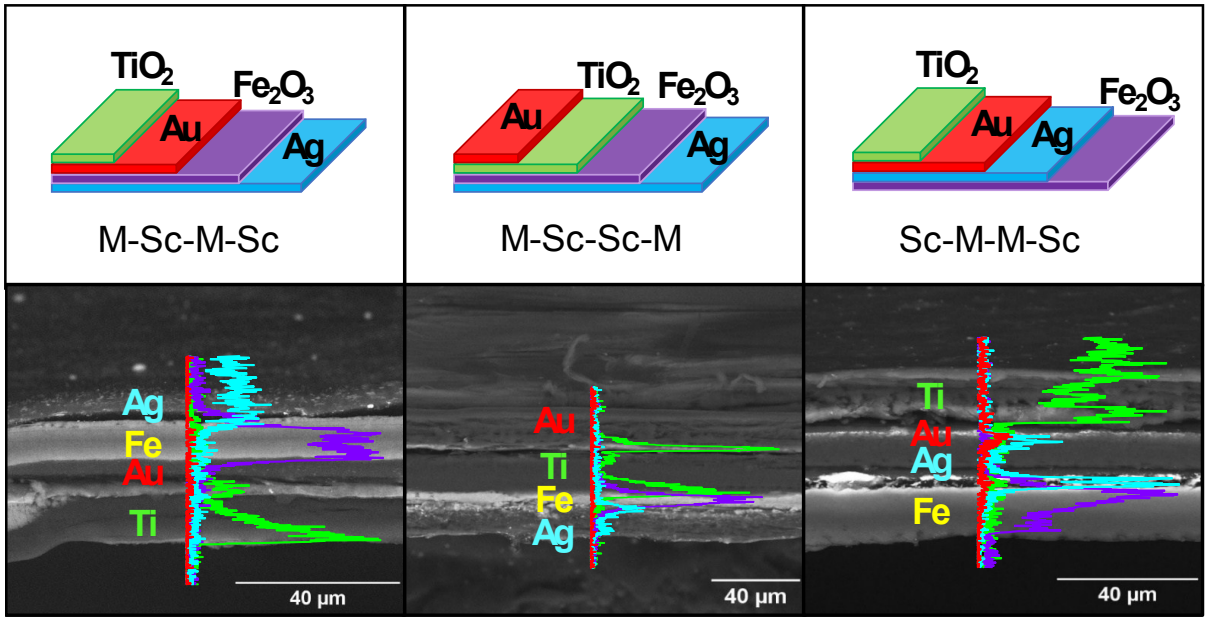

Figure S4. Different conformations of a laminated millefeuille construction with its particular cross section SEM image. An EDX line scan was done to confirm the space distribution of the nanoparticles. M: metal, Sc: semiconductor. Metal contribution was smaller in these constructs as the precursor concentration was ten times lower than semiconductors precursors.

Figure S5. Videos showing the mechanical properties of a laminated multifunctional bacterial cellulose millefeuille. A) Tensile test B) Flexibility of the material after drying. C) Flexibility of the material after rewetting.

References:

1 M. Zeng, A. Laromaine, W. Feng, P. A. Levkin and A. Roig, *J. Mater. Chem. C*, 2014, **2**, 6312–6318.

2 J. C. Phillips, R. Braun, W. Wang, J. Gumbart, E. Tajkhorshid, E. Villa, C. Chipot, R. D. Skeel, L. Kalé and K. Schulten, *J. Comput. Chem.*, 2005, **26**, 1781–1802.

3 T. C. F. Gomes and M. S. Skaf, *J. Comput. Chem.*, 2012, **33**, 1338–1346.

4 O. Guvench, S. S. Mallajosyula, E. P. Raman, E. Hatcher, K. Vanommeslaeghe, T. J. Foster, F. W. Jamison and A. D. MacKerell, *J. Chem. Theory Comput.*, 2011, **7**, 3162–3180.

5 J. L. F. Abascal and C. Vega, *J. Chem. Phys.*, 2005, **123**, 234505.

6 C. Vega and J. L. F. Abascal, *Phys. Chem. Chem. Phys.*, 2011, **13**, 19663–19688.

7 C. Calero, J. Martí and E. Guàrdia, *J. Phys. Chem. B*, 2015, **119**, 1966–1973.

8 J. Hénin, G. Fiorin, C. Chipot and M. L. Klein, *J. Chem. Theory Comput.*, 2010, **6**, 35–47.

9 V. Sashuk and K. Rogaczewski, *J. Nanoparticle Res.*, 2016, **18**, 261.

10 C. E. Hoppe, M. Lazzari, I. Pardiñas-Blanco and M. A. López-Quintela, *Langmuir*, 2006, **22**, 7027–7034.

11 S.-H. Jeon, P. Xu, N. H. Mack, L. Y. Chiang, L. Brown and H.-L. Wang, *J. Phys. Chem. C*, 2010, **114**, 36–40.

12 R. Deshmukh and M. Niederberger, *Chem. - A Eur. J.*, 2017, **23**, 8542–8570.

13 M. Niederberger and G. Garnweitner, *Chem. - A Eur. J.*, 2006, **12**, 7282–7302.